# AN ANALYTICAL MODEL FOR THE DETERMINATION OF DISC EDGE VORTEX STRENGTH, LOCATION AND GEOMETRY AT LOW TO INTERMEDIATE FLYING SPEEDS

J.P. Roos
Delft University of Technology
Faculty for Aerospace Engineering
Delft, the Netherlands

## Abstract

During forward flight the main rotor wake rolls up into two disc edge vortices, comparable to the tip vortices behind a wing. At low to intermediate flying speeds (≥ 35 knots), these vortices dominate the flow at the tail rotor and tail planes, therefore affecting their performance and in turn helicopter stability and control. To predict and simulate the influence of these vortices, an analytical model has been developed to determine their location, strength and geometry.

From previous research it can be concluded that the disc edge vortices form, when the cylindrical rotor wake degenerates into an approximately flat vortex sheet. The distribution of vorticity inside this sheet has been determined and it is concluded that it is equivalent to the wake behind a wing. The rotor is replaced by an equivalent wing and the circulation distribution along its span is calculated. Finally, the rolling up motion of the wake is analyzed with a classical fixed wing theory.

The verification included in this paper shows a satisfactory agreement, but more experimental data is needed to verify the model for advance ratios below $\mu$=0.15. For this reason a small scale helicopter wind tunnel model is being developed, however test results where not available in time for this publication.

## Notations

### Symbols

| | | |
|---|---|---|
| b | number of blades | |
| $C_T$ | rotor thrust coefficient, $C_T=T/\pi R^2\rho V_t^2$ | |
| D | helicopter drag | [N] |
| e | distance behind the rotor where a disc edge vortex is fully formed | [m] |
| $\bar{e}$ | non-dimensional distance behind the rotor where a disc edge vortex is fully formed, $\bar{e}=e/R$ | |
| R | rotor radius | [m] |
| r, $\varphi$ | polar coordinates | [m],[rad] |
| $\bar{r}$ | non-dimensional radial distance; $\bar{r}=r/R$ | |
| T | rotor thrust | [N] |
| t | time | [s] |
| $u_t$ | tangential velocity inside disc edge vortex | [m/s] |
| V | velocity or flying speed | [m/s] |
| $V_t$ | tip speed; $V_t=\Omega R$ | [m/s] |
| $v_i$ | rotor or vortex induced velocity | [m/s] |
| W | helicopter weight | [N] |
| x, y, z | Cartesian coordinates | [m] |
| $\bar{x}$, $\bar{y}$, $\bar{z}$ | non-dimensional Cartesian coordinates; $\bar{x}=x/R$, $\bar{y}=x/R$, $\bar{z}=z/R$ | |
| $\alpha$ | angle of attack | [rad] |
| $\Gamma$ | circulation | [$m^2$/s] |
| $\gamma$ | circulation per unit length or vorticity | [m/s] |
| $\mu$ | advance ratio; $\mu=V\cos\alpha_d/V_t$ | |
| $\zeta$, $\eta$ | Cartesian coordinates | [m] |
| $\bar{\zeta}$, $\bar{\eta}$ | non-dimensional Cartesian coordinates; $\bar{\zeta}=\zeta/R$, $\bar{\eta}=\eta/R$ | |
| Z | length of the vortex sheet that has rolled up into a disc edge during time t | [m] |
| $\bar{Z}$ | non-dimensional length of the vortex sheet that has rolled up into a disc edge vortex during time t | |
| $\kappa$ | constant in circulation distribution | [$m^{3/2}$/s] |
| $\rho$ | air density | [kg/$m^3$] |
| $\chi$ | wake skew angle | [rad] |
| $\psi$ | blade azimuth angle | [rad] |
| $\Omega$ | rotor rotational velocity | [rad/s] |

### Subscripts

| | |
|---|---|
| adv | advancing side |
| c | center of vortex or circular |
| cg | center of gravity |
| d | disc |
| l | longitudinal |
| retr | retreating side |
| s | shed |
| t | tip or tangential |

## 1 Introduction

The vortex system shed from a helicopter rotor in forward flight rolls up rapidly downstream of the aircraft to form two, oppositely rotating vortices. These disc edge vortices are strong and large, capable to engulf the tail rotor during a direct interaction. Therefore strongly affecting helicopter directional control and handling qualities [1,2,3]. As is illustrated by the sudden pedal motions needed to control the aircraft at certain yaw angles to the left and right [4,5].

In the present work a model is derived to determine the strength, location and geometry of the disc edge vortices. It will be used in the future to simulate their influence on helicopter directional control. A verification of the results obtained with the model is also included in this paper.

## 2 Derivation of the model

### 2.1 Observed rotor wake - wing wake equivalence

The basic mechanism of the rolling up process of the rotor wake is similar to that which causes the formation of the well-known tip vortices trailing behind a fixed wing. This process is more easily visualised in terms of the rolling up of an imaginary cylinder, outlined by the helical blade tip vortices moving downstream. This is illustrated by figure 1, used by Landgrebe & Bellinger [6] to explain the distortions of blade tip vortices seen in the experiment of Lehman [7].

This similarity between a rotor and a fixed wing also appears in momentum theory, from which it is known that the rotor of the average helicopter starts to act as a circular wing, for flying speeds somewhere between 25 and 35 knots. Experiments show that disc edge vortex formation is indeed evident within this range [1,2,5,7].

The model derived here will be based on the similarity indicated above. The undisturbed rotor wake will be redefined as an equivalent fixed wing wake, with the help of a flat wake theory developed by Ormiston [10]. It should be noted that Ormiston states that this theory should not be used for the calculation of induced velocities at the rotor disc, below an advance ratio of $\mu$=0.15. Which is substantiated by [7,8,9], where it can be seen that the cylindrical character of the wake starts to prevail directly below the rotor. The same experiments show however that the wake behind the rotor still has a wing like character. This may be explained by the fact that the cylindrical wake not only skews back but also contracts. At some distance behind the rotor its wake will therefore still degenerate into an approximately flat vortex sheet.

For the present purpose it is therefore assumed that the flat wake concept remains approximately valid for advance ratios below the mentioned limit. Hopefully covering the total range where the disc edge vortices are of interest.

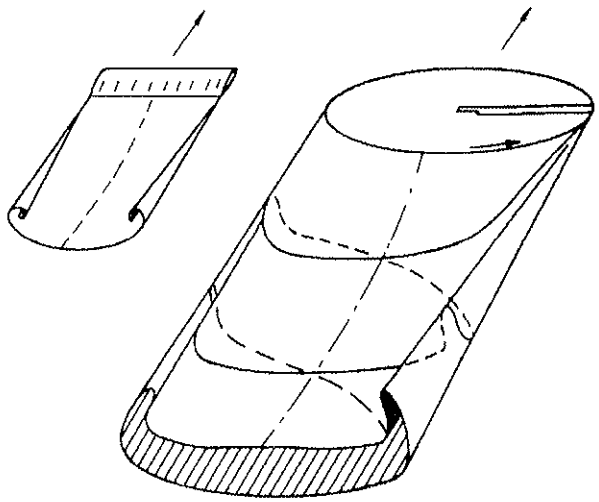

**Figure 1: Rolling up of a rotor and fixed wing wake [6]**

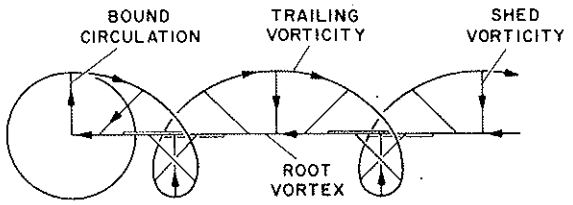


**Figure 2: Elements of vorticity inside the flat wake [10]**

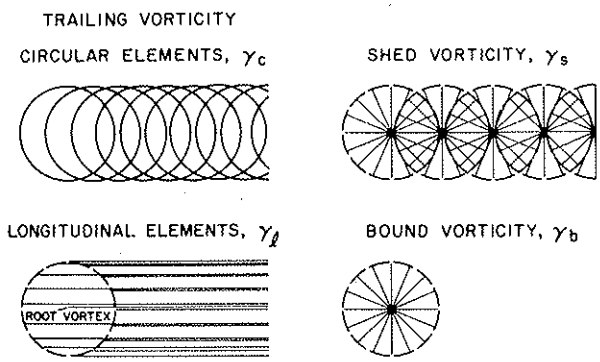


**Figure 3: Decomposition of the flat wake [10]**

### 2.2 Redefinition of the rotor wake as a wing wake

Ormiston [10] derived his flat wake theory in order to simplify the calculation of induced velocities at the rotor disc. It is based on the idea that the helical wake behind the rotor can be decomposed into a number of simple vortex patterns, see figures 2 and 3. Note that when the circulation along a blade is finite at the blade root, the root vortices combine into a discrete vortex having its starting point in the rotor center.

When in turn, these structures are resolved into lateral (subscript y) and longitudinal (subscript x) vorticity components, the following result is obtained. Provided that the distribution of circulation over the rotor disc is symmetric with respect to its lateral axis, summation of vorticity generated by the front and aft of the disc causes the lateral vorticity component $\gamma_y$, to disappear. The flat wake therefore only contains vorticity in the longitudinal direction $\gamma_x$, which makes it totally equivalent to that trailing behind a wing.

Before the flat rotor wake can be redefined as a wing wake, the variation of the circulation, bound by a blade, has to be determined.

Due to the rapid formation of the blade tip vortices, it seems as if they trail from a blade with constant circulation

along its span. It is therefore assumed that the only variation that needs to be considered is the azimuthal change of the blade circulation $\Gamma(\psi)$, which is expressed through a Fourier-series. Consequently, the blade wake will consist of a root vortex, tip vortex and a sheet of shed vorticity. Finally, since only rotor trim is considered here, i.e., the rotor should be in moment equilibrium and develop enough thrust T to balance helicopter weight and drag, the series is truncated at the first order sin term, see Meijer Drees[11]:

$$\Gamma = \Gamma_0 + \Gamma_1 \sin\psi, \tag{1}$$

the two constants $\Gamma_0$ and $\Gamma_1$ can be found by evaluating the trim conditions mentioned above. For the used signs and notations, see figure 4. Meijer Drees derived the following result for a centrally hinged rotor with no hinge offset or root cut out;

$$\Gamma_0 = \frac{2T}{b\rho R V_t\left(1 - \frac{3}{2}\mu^2\right)} \tag{2}$$

and

$$\Gamma_1 = -\frac{3}{2}\mu\Gamma_0, \tag{3}$$

where b denotes the number of blades, $\rho$ the air density, R the rotor radius and finally $V_t$ the tip speed of a rotor blade. Since the disc angle of attack is small in low speed forward flight, $\alpha_d \ll 1$ rad, the advance ratio $\mu$ in equation (2) and (3) can be approximated by;

$$\mu = \frac{V\cos(\alpha_d)}{V_t} \approx \frac{V}{V_t}. \tag{4}$$

The distribution of circulation over the rotor disc, given by equation (1), is symmetric with respect to its lateral axis of symmetry, which means that the redefined wake consists of longitudinal vorticity components $\gamma_x$ and an additional discrete root vortex. Ormiston gives the following result;

$$\gamma_x = \gamma_1 + \gamma_{c_x} + \gamma_{s_x}, \tag{5}$$

where the three vorticity components on the right-hand side can be found in table 2 of reference [10], see figure 3 for their definition:

$$\gamma_1 = \frac{1}{\pi R}\frac{\Gamma_0 + \Gamma_1\bar{y}}{\sqrt{1-\bar{y}^2}}$$

$$\gamma_{c_x} = \frac{1}{\pi\mu R}\frac{(\Gamma_0 + \Gamma_1\bar{y})\bar{y}}{\sqrt{1-\bar{y}^2}} \tag{6}$$

$$\gamma_{s_x} = \frac{1}{\pi\mu R}\Gamma_1\left[\sqrt{1-\bar{y}^2} - \ln\left(\frac{1+\sqrt{1-\bar{y}^2}}{|\bar{y}|}\right)\right],$$

in which $\bar{y}$ denotes the non-dimensional lateral coordinate of a point inside the wake, defined as $\bar{y}=y/R$. Note that, equation (7) gives the distribution of vorticity due to one blade, when the constants in equation (1) are defined by equations (2) and (3). To take the contribution of all rotor blades into account, equation (2) should therefore be multiplied by b. For the actuator disc $\Gamma_0$ is thus given by;

$$\Gamma_0 = \frac{2T}{\rho R V_t\left(1 - \frac{3}{2}\mu^2\right)}, \tag{7}$$

while $\Gamma_1$ is still given by equation (3).

In the next paragraph the rotor wake will be looked upon as generated by an equivalent circular wing. Equations (5) and (6) can then be used to calculate the distribution of circulation along its span.

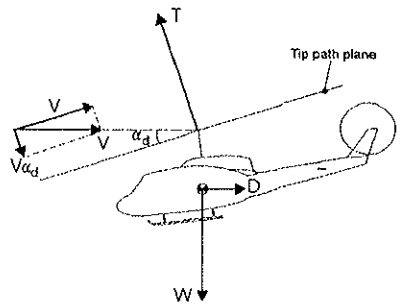


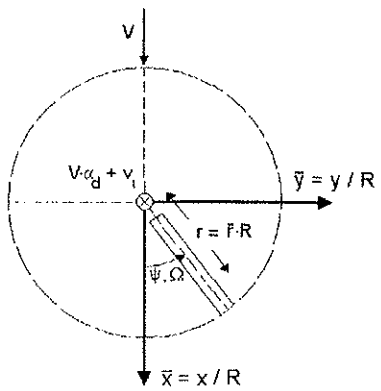


**Figure 4: Signs and notations, part 1**

2.2 Circulation along an equivalent circular wing

The determination of the distribution of circulation along the span of the equivalent circular wing is a straight forward matter. It follows after integration of all the vorticity components, determined in the previous paragraph;

$$\Gamma(\bar{y}) = -R\int\gamma(\bar{y})d\bar{y}. \tag{8}$$

Performing the indicated integrations, gives for the contribution of trailing vorticity components;

$$\Gamma_{c_x} = \frac{1}{\pi\mu}\left(\Gamma_0\sqrt{1-\bar{y}^2} + \frac{1}{2}\Gamma_1\left[\bar{y}\sqrt{1-\bar{y}^2} - \arcsin\bar{y}\right]\right), \tag{9}$$

and

$$\Gamma_1 = \frac{1}{\pi}\left(-\Gamma_0 \arcsin \bar{y} + \Gamma_1\sqrt{1-\bar{y}^2}\right), \qquad (10)$$

while for the contribution of the shed components is found;

$$\Gamma_{s_x} = \frac{1}{\pi\mu}\Gamma_1\left(\bar{y}\ln\left[\frac{1+\sqrt{1-\bar{y}^2}}{|\bar{y}|}\right] + \frac{1}{2}\arcsin\bar{y} - \frac{1}{2}\bar{y}\sqrt{1-\bar{y}^2}\right). \qquad (11)$$

Finally, the distribution of circulation along the wing span is given by;

$$\Gamma = \Gamma_{0_x} + \Gamma_1 + \Gamma_{s_x} \qquad (12)$$

and is shown in figure 5.

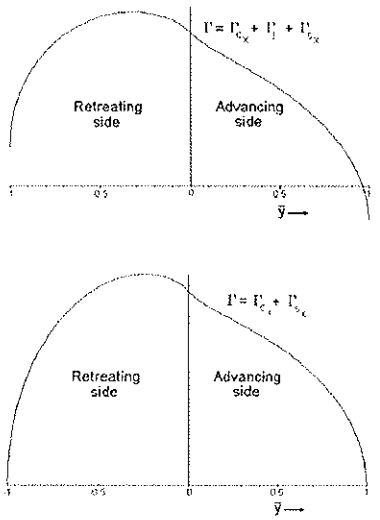


**Figure 5: Circulation along an equivalent circular wing**

From this figure it can be seen that the circulation does not equal zero at the wing tips, suggesting the presence of two discrete vortices. This is a direct consequence of the time averaged modeling of the wake, which can be corrected for by introducing a lift deficiency function. However, such a function is not known, so the contribution of the longitudinal circulation components $\Gamma_1$ and in addition the root vortex are neglected instead. Although primarily to obtain a correct circulation distribution, again see figure 5, this has an other reason as well. Since the corrected wake is similar to that used by Meijer Drees [11], his well-known inflow model can be used to find the downward displacement of both disc edge vortices. Acceptance of this simplification leads to the following circulation distribution;

$$\Gamma = \frac{1}{\pi\mu}\Gamma_0\left(\sqrt{1-\bar{y}^2} - \frac{3}{2}\mu\bar{y}\ln\left[\frac{1+\sqrt{1-\bar{y}^2}}{|\bar{y}|}\right]\right), \qquad (13)$$

It should be noted that quite recently a free wake model has been developed by Bühler & Newman [12], based on similar assumptions as where made in the present work. Blade circulation was taken constant along the span and varying with the azimuth according to eq. (1). The wake was initially assumed to be flat and approximated by vortex rings, the latter where free to distort and thus not confined to their initial circular shape. The only differences, the present model is a time averaged one and finally Bühler & Newman neglect the shed components of vorticity.

The computed roll up motion of this wake seems to capture the trends described by Ghee & Elliot [9], which might be seen as a further substantiation of the simplifying assumptions made till now.

2.3 Disc edge vortex formation

Now the rotor wake has been redefined as a wing wake, it is allowed to roll up into the two disc edge vortices. The strength, location and geometry of which will be determined with a classical fixed wing theory developed by Kaden [13]. For more information about this elaborate theory, the reader is referred to the original paper.

Kaden investigated the rolling up of a vortex sheet of semi-infinite width. His results are therefore only applicable to a vortex sheet of finite width for the initial stages of the rolling up process. In addition, it should be noted that the semi-infinite sheet has no downward motion. Spreitner & Sacks [14], however showed that Kaden's solution is useful in the formulation of some further approximations to the paths of the vortex cores and the distance needed for them to become essentially rolled up. Finally, to incorporate Kaden's results in the present model, the coordinate $\zeta$ is introduced. This coordinate runs opposit along the x-axis and equals zero at the edge of the sheet, see figure 6.

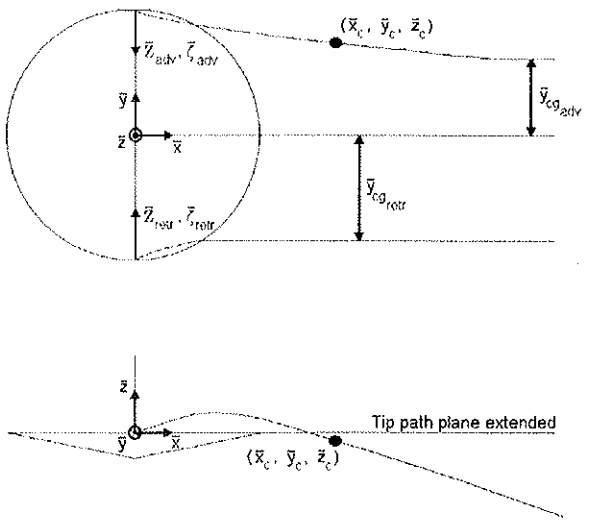


**Figure 6: Signs and notations, part 2**

Kaden derived his model based on the following circulation distribution;

$$\Gamma = 2\kappa\sqrt{\zeta} = 2\kappa\sqrt{R}\sqrt{\bar{\zeta}}, \qquad (14)$$

where the non-dimensional coordinate $\bar{\zeta}$ is defined as $\bar{\zeta} = \zeta/R$. This distribution can be related to the one that is currently under investigation, near the edges of the wake, by finding the factor $\kappa$ for both the advancing (subscript adv) and retreating side (subscript retr).

The calculation will be illustrated for the advancing side. Substitution of $\bar{y}=1-\bar{\zeta}$ in equation (13) gives;

$$\Gamma = \frac{1}{\pi\mu}\Gamma_0\left(\sqrt{\bar{\zeta}}\sqrt{2-\bar{\zeta}^2} - \frac{3}{2}\mu(1-\bar{\zeta})\ln\left[\frac{1+\sqrt{\bar{\zeta}}\sqrt{1-\bar{\zeta}^2}}{|\bar{\zeta}|}\right]\right).$$

For very small $\bar{\xi}$ this can be approximated by;

$$\Gamma = \frac{1}{2}\sqrt{2}(1-\frac{3}{2}\mu)\sqrt{\bar{\zeta}}, \qquad (15)$$

finally, equating this result to equation (14) and solving for $\kappa$ gives;

$$\kappa_{adv} = \frac{1}{2}\sqrt{2}\frac{1}{\pi\mu\sqrt{R}}\Gamma_0(1-\frac{3}{2}\mu). \qquad (16)$$

Similarly, substitution of $\bar{y}=\bar{\zeta}-1$ gives for the retreating side;

$$\kappa_{retr} = \frac{1}{2}\sqrt{2}\frac{1}{\pi\mu\sqrt{R}}\Gamma_0(1+\frac{3}{2}\mu). \qquad (17)$$

This difference between the advancing and retreating side will cause an asymmetry in every aspect of the rolled up wake. These asymmetries grow with increasing advance ratio.

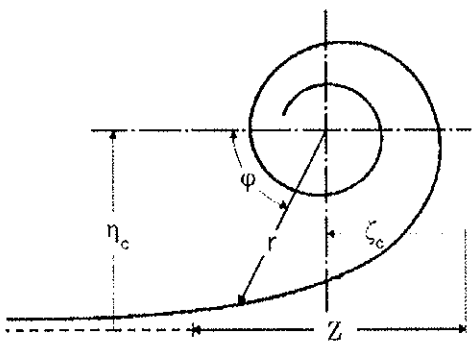


**Figure 7: Signs and notations, part 3**

Kaden deduced that the lateral coordinates of the centers of the developing vortices, see figure 7, are given by;

$$\zeta_0 = 0.57Z,$$
$$\eta_c = 0.88Z, \qquad (18)$$

where Z denotes the length of the part of the sheet that has rolled up into the vortices till time t, measured from the start of the rolling up process;

$$Z = \left(\frac{9}{2\pi^2}\kappa t\right)^{\frac{2}{3}}. \qquad (19)$$

In steady forward flight the vortices are transported away from the rotor with the freestream velocity, time can therefore be related to the non-dimensional distance behind the rotor $x_c=x_c/R$ as;

$$\bar{x}_0 = \frac{Vt}{R} \quad \text{or} \quad t = \frac{R\bar{x}_0}{V}. \qquad (20)$$

Substitution of this and the correct value of $\kappa$ into equation (19) gives, for the advancing and retreating side respectively;

$$\bar{Z}_{adv} = R^{-\frac{1}{3}}\left(\frac{9}{2\pi^2}\kappa_{adv}\frac{\bar{x}_0}{V}\right)^{\frac{2}{3}},$$
$$\bar{Z}_{retr} = R^{-\frac{1}{3}}\left(\frac{9}{2\pi^2}\kappa_{retr}\frac{\bar{x}_0}{V}\right)^{\frac{2}{3}}. \qquad (21)$$

2.4 Disc edge vortex lateral location

In the tip path plane bound coordinate system used here, the lateral location of each disc edge vortex is determined by, see equation (18) and figure 6;

$$\bar{y}_{c_{adv}} = 1 - 0.57\bar{Z}_{adv}$$
$$\bar{y}_{c_{retr}} = 0.57\bar{Z}_{retr} - 1 \qquad (22)$$

This equation shows that the lateral coordinate $\bar{y}_c$ of both vortices does not approach an asymptote. Consequently, Spreitner and Sacks proposed to use Kaden's solution till the asymptotes are reached, with which the disc edge vortices are assumed to coincide from then on.

The location of the asymptotes follows from the condition that the impulse of the vortex system is preserved during the rolling up process. This then leads to the conclusion that a fully formed vortex must coincide with the center of gravity of the part of the sheet from which it originates. Note that this rule is well known for its prediction of the distance between the two tip vortices behind an elliptical wing, which is found to be $\pi/4$ times the wing span.

The location of the asymptotes can be calculated, when it is known which part of the vortex sheet rolls up into the advancing and retreating vortex respectively.

The elementary vortices inside the sheet change their direction at the point where the circulation distribution reaches its maximum. To the left of this point the sheet will roll up into the retreating and the part to the right into the advancing disc edge vortex. The location of this maximum can be found by differentiating equation (13) with respect to y and setting the result equal to zero. However, this equality can only be solved in an iterative way, the results of this calculation are given in table 1.

The location of the centers of gravity on both the advancing and retreating side can now be determined with;

$$\bar{y}_{cg} = \frac{y_{cg}}{R} = \frac{1}{R}\frac{\int\frac{\partial\Gamma}{\partial y}y\,dy}{\int\frac{\partial\Gamma}{\partial y}dy} = \frac{\int\frac{\partial\Gamma}{\partial\bar{y}}\bar{y}\,d\bar{y}}{\int\frac{\partial\Gamma}{\partial\bar{y}}d\bar{y}}.$$

The integration limits are: for the part of the sheet that rolls up into the retreating side disc edge vortex -1 ; y ;($\Gamma=\Gamma_{max}$)

and for the advancing disc edge vortex $\bar{y}(\Gamma = \Gamma_{max}) < \bar{y} \leq 1$. Again, the results are given in table 1.

**Table 1: Centers of gravity, point of max. circulation**

| $\mu$ | $\bar{y}(\Gamma = \Gamma_{max})$ | $\bar{y}_{cG\,retr}$ | $\bar{y}_{cG\,adv}$ |
|---|---|---|---|
| 0.09 | -0.182 | -0.821 | 0.687 |
| 0.10 | -0.193 | -0.823 | 0.675 |
| 0.11 | -0.203 | -0.825 | 0.663 |
| 0.12 | -0.212 | -0.827 | 0.651 |
| 0.13 | -0.221 | -0.829 | 0.639 |
| 0.14 | -0.230 | -0.831 | 0.627 |
| 0.15 | -0.238 | -0.833 | 0.615 |
| 0.16 | -0.245 | -0.835 | 0.603 |
| 0.17 | -0.252 | -0.837 | 0.592 |
| 0.18 | -0.259 | -0.838 | 0.580 |
| 0.19 | -0.265 | -0.840 | 0.569 |
| 0.20 | -0.271 | -0.841 | 0.557 |
| 0.21 | -0.277 | -0.842 | 0.546 |
| 0.22 | -0.283 | -0.844 | 0.535 |
| 0.23 | -0.288 | -0.845 | 0.523 |
| 0.24 | -0.293 | -0.846 | 0.512 |

For the advancing side, the point where Kaden's solution intersects the asymptote is determined by the condition that;

$$\bar{y}_{cg_{adv}} = 1 - 0.57\,\bar{Z}_{adv},$$

denoting the intersection by $\bar{s}_{adv}$ and substitution of equation (21) gives;

$$\bar{s}_{adv} = \frac{2}{9}\pi^2 R \left( \frac{1}{0.57}\left(1 - \bar{y}_{cg_{adv}}\right)\right)^{\frac{3}{2}} \frac{V}{\kappa_{adv}}. \qquad (23)$$

Similar reasoning gives for the retreating side;

$$\bar{s}_{retr} = \frac{2}{9}\pi^2 R \left( \frac{1}{0.57}\left(1 + \bar{y}_{cg_{retr}}\right)\right)^{\frac{3}{2}} \frac{V}{\kappa_{retr}}. \qquad (24)$$

From these points onwards the location of the disc edge vortices is thus given by;

$$\begin{aligned} \bar{y}_{c_{adv}} &= \bar{y}_{cg_{adv}} \quad \text{for} \quad \bar{x} \geq \bar{s}_{adv} \\ \bar{y}_{c_{retr}} &= \bar{y}_{cg_{retr}} \quad \text{for} \quad \bar{x} \geq \bar{s}_{retr} \end{aligned} \qquad (25)$$

2.5 Disc edge vortex axial location

As stated before, the semi-infinite sheet used by Kaden does not have a downward motion. His theory therefore only describes the upward motion of the vortex, with respect to the flat vortex sheet, see figure 7 and equation (18):

$$\begin{aligned} \bar{z}_{c_{adv}} &= 0.88\,\bar{Z}_{adv} \\ \bar{z}_{c_{retr}} &= 0.88\,\bar{Z}_{retr} \end{aligned} \qquad (26)$$

This can be corrected by using yet an other reflection of Spreitner and Sacks. They stated that the downward motion of the tip vortices behind an elliptical wing can be determined within narrow limits, when the following is assumed. Close to the wing the vortices move downward with a constant velocity, equal to that induced at the center of gravity of each sheet half and at some distance behind it, with the velocity that the fully formed vortices impart on each other.

In accordance with the wing analogy, the flat wake is assumed to leave the rotor at its trailing edge. The velocity with which it moves downward can be determined with the inflow model, developed by Meijer Drees [11]. The induced velocity distribution over the rotor disc is considered first;

$$v_i = \frac{C_T}{2\mu\left(1 - \frac{3}{2}\mu^2\right)} V_t \left[ 1 - \cos\chi + \tfrac{4}{3}\left(1 - 1.8\mu^2\right)\bar{r}\cos\psi - 2\mu\bar{r}\sin\chi\sin\psi \right].$$

It can be seen from this equation that the average induced velocity is not equal to that induced by a circular wing. According to Heyson [15] this should be corrected by disregarding the term $(1-3/2\mu^2)$. Furthermore, for the flat wake the skew angle equals $\chi = 1/2\pi$, while at the trailing edge $r = r/R = 1$, $y = \sin\psi$, and $\cos\psi = \sqrt{(1-y)}$. Substitution of this gives;

$$v_i = \frac{C_T}{2\mu} V_t \left[ 1 + \tfrac{4}{3}\left(1 - 1.8\mu^2\right)\sqrt{1 - \bar{y}^2} - 2\mu\bar{y} \right]. \qquad (27)$$

Finally, since the tip path plane is taken as a reference, the small perpendicular component of the flying speed has to be considered. Adding this to equation (27) gives the downward velocity at the trailing edge $v_d$;

$$v_d = \frac{C_T}{2\mu} V_t \left[ 1 + \tfrac{4}{3}\left(1 - 1.8\mu^2\right)\sqrt{1 - \bar{y}^2} - 2\mu\bar{y} \right] + V\alpha_d. \qquad (28)$$

The downward velocity of both the advancing and retreating side vortex follows from this equation, after substitution of the correct value for $y_{cg}$ from table 1.

Now the downward velocity of the fully formed disc edge vortices will be determined. Each vortex may be regarded as fully rolled up, when it encloses the full width of the sheet out of which it forms. For the advancing side, this translates into;

$$\bar{Z}_{adv} = 1 - \bar{y}(\Gamma = \Gamma_{max}), \qquad (29)$$

denoting the distance behind the rotor, where the vortex is fully formed, by $x = e_{adv}$ and introducing $\bar{e}_{adv} = e_{adv}/R$, then substitution of equation (21) into equation (29) gives, after some rearranging;

$$\bar{e}_{adv} = \frac{2}{9}\pi^2 R \left(1 - \bar{y}(\Gamma = \Gamma_{max})\right)^{\frac{3}{2}} \frac{V}{\kappa_{adv}}. \qquad (30)$$

Following the same approach gives for the retreating side;

$$\bar{e}_{retr} = \frac{2}{9}\pi^2 R \left(1 + \bar{y}(\Gamma = \Gamma_{max})\right)^{\frac{3}{2}} \frac{V}{\kappa_{retr}}. \qquad (31)$$

From table 1 and equations (30) and (31) it can be seen that the distance needed for the retreating side vortex to roll up

is smaller than that for the advancing side vortex. The approach, proposed by Spreitner and Sacks is therefore slightly adapted. Once the retreating side disc edge vortex is fully rolled up, it is assumed to move downwards with the velocity it would have at some great distance behind the rotor, where both vortices are fully formed. This downward velocity (subscript $\infty$) can be found with the Biot-Savart Law;

$$v_{d_\infty} = \frac{\Gamma_{max}}{2\pi(y_{cg_{adv}} - y_{cg_{retr}})} = \frac{\Gamma_{max}}{2\pi R(\bar{y}_{cg_{adv}} - \bar{y}_{cg_{retr}})}, \qquad (32)$$

where $\Gamma_{max}$ can be determined with equation (13) and table 1.

The axial location of both disc edge vortices is now approximately known. Near the rotor;

$$\bar{z}_{c_{adv}} = 0.88\bar{Z}_{adv} - \frac{v_{d_{adv}}}{V}\bar{x} \quad \text{for} \quad \bar{x} \le \bar{e}_{adv}$$
$$\bar{z}_{c_{retr}} = 0.88\bar{Z}_{retr} - \frac{v_{d_{retr}}}{V}\bar{x} \quad \text{for} \quad \bar{x} \le \bar{e}_{retr} \qquad (33)$$

and when the disc edge vortices are fully rolled up;

$$\bar{z}_{c_{adv}} = \bar{z}_{c_{adv}}(\bar{x} = \bar{e}_{adv}) - \frac{v_{d_\infty}}{V}(\bar{x} - \bar{e}_{adv}) \quad \text{for} \quad \bar{x} > \bar{e}_{adv}$$
$$\bar{z}_{c_{retr}} = \bar{z}_{c_{retr}}(\bar{x} = \bar{e}_{retr}) - \frac{v_{d_\infty}}{V}(\bar{x} - \bar{e}_{retr}) \quad \text{for} \quad \bar{x} > \bar{e}_{retr} \qquad (34)$$

## 2.6 Disc edge vortex strength

The strength of the disc edge vortices is reflected in the circulation distribution, and therefore follows from equation (13). Substitution of $y=1-Z_{adv}$ for the advancing and $y=Z_{retr}-1$ for the retreating side vortex gives;

$$\Gamma_{c_{adv}} = \frac{\Gamma_0}{\pi\mu}\left(\sqrt{1-(1-\bar{Z}_{adv})^2} - \frac{3}{2}\mu(1-\bar{Z}_{adv})\ln\left(\frac{1+\sqrt{1-(1-\bar{Z}_{adv})^2}}{|1-\bar{Z}_{adv}|}\right)\right), \qquad (35)$$

$$\Gamma_{c_{retr}} = \frac{\Gamma_0}{\pi\mu}\left(\sqrt{1-(\bar{Z}_{retr}-1)^2} - \frac{3}{2}\mu(\bar{Z}_{retr}-1)\ln\left(\frac{1+\sqrt{1-(\bar{Z}_{retr}-1)^2}}{|\bar{Z}_{retr}-1|}\right)\right).$$

After the rolling up process is completed, the strength of both vortices equals $\Gamma_{max}$, which can be obtained by substitution of the correct value for $y(\Gamma=\Gamma_{max})$ into equation (13), see table 1.

## 2.7 Disc edge vortex geometry and internal velocities

The spiral that represents the shape of a cross-section of a disc edge vortex is given by Kaden as, see also figure 7;

$$r = \left(\frac{3}{2}\right)^{\frac{1}{3}}\left(\frac{\kappa t}{\pi\varphi}\right)^{\frac{2}{3}}, \qquad (36)$$

where r and $\varphi$ are polar coordinates in a coordinate system with an origin that coincides with the center of a disc edge vortex, see figure 9. The limits for $\varphi$ are $1/2 \le \varphi \le \infty$ where the point $\varphi = 1/2\pi$ corresponds to $r = R_0$, which is assumed to be the vortex outer radius. Note that, for the case of fully formed tip vortices behind an elliptical wing, the dimensions predicted by equation (36), are approximately the same as predicted by Prandtl, see Durand [16]. The largest component in the current circulation distribution is also elliptic, see equation (13), therefore one may expect that equation (36) gives reasonable results. This is further substantiated by the fact that in Kaden's theory geometry and location of the vortices are closely connected. Since it predicts the location of the tip vortices behind a wing well the same must be true for their geometry.

It must be noted that equation (36) is defined in a coordinate system that only matches the advancing side. To be able to draw the cross-sections of both disc edge vortices in the coordinate system used here, the following is written;

$$\bar{y}_{w_{adv}} = \bar{y}_{c_{adv}} - \bar{r}_{adv}\cos\varphi, \quad \bar{z}_{w_{adv}} = \bar{z}_{c_{adv}} - \bar{r}_{adv}\sin\varphi;$$
$$\bar{y}_{w_{retr}} = \bar{y}_{c_{retr}} + \bar{r}_{retr}\cos\varphi, \quad \bar{z}_{w_{retr}} = \bar{z}_{c_{retr}} - \bar{r}_{retr}\sin\varphi, \qquad (37)$$

where $\bar{r} = r/R$. Note that equation (37) is given in a general form, to apply it to the advancing side and retreating side disc edge vortex, the correct value for $\kappa$ should be substituted.

Finally, the distribution of velocities inside both vortices is considered, which is convenient for the calculation of tail rotor thrust and tail plane lift during an interaction. This distribution is given by;

$$u_t = \sqrt{\frac{3}{2}\frac{\kappa}{\pi\sqrt{r}}} \qquad (38)$$

Kaden derived this formula, based on his observation that the inner most windings of the spiral are approximately circular in shape. Because of this, he concludes that the radial component of the internal velocity disappears and that only the tangential component remains (subscript t). In other words the velocities are directed perpendicular to r, given by equation (36).

Though strictly valid for its inner region, it is assumed that this equation is approximately valid for the whole spiral. The reason, this velocity distribution belongs to a vortex cross-section as described by equation (36), for which it was already debated that it must be a reasonable approximation.

## 3 Verification of the model

Sources that provide data for a verification are Heyson [8] and Ghee & Elliot [9]. However, Heyson gives vorticity plots at only three stations behind the rotor, not enough for a satisfactory comparison. These results will therefore not be used. For a further verification the Faculty of Aerospace Engineering, of the Delft University of Technology (DUT),

is developing a small scale helicopter model. The funding for which is provided by both the DUT and the Dutch National Aerospace Laboratory (NLR). Test results are expected soon and the following comparison with Ghee & Elliot is therefore of a preliminary nature.

3.1 Description of the experiment, Ghee & Elliot [9]

The experimental investigation, used here for the verification, was conducted by Ghee and Elliot in the 14 by 22-foot Subsonic Tunnel at NASA Langley Research Center. Which was used in the open section configuration. They quantified the wake behind a scale model rotor for two advance ratios, $\mu$=0.15 and $\mu$=0.23, and one thrust level $C_T$=0.0064.

For the experiments a 2 m diameter, four bladed, articulated rotor system was used with a generic fuselage. The rotor hub incorporated coincident flap and lead-lag hinges that employed viscous lag dampers. Details of this rotor are given in table 2.

**Table 2: Details of the rotor [9]**

| | | |
|---|---|---|
| Hub type | Articulated | |
| Number of blades | 4 | |
| Airfoil section | NACA 0012 | |
| Hinge offset, r/ R | 0.06 | |
| Root cutout, r/ R | 0.24 | |
| Linear twist, deg | -8 | |
| Radius | 0.861 | m |
| Airfoil chord | 0.066 | m |
| Rotor solidity, $\sigma = bc/\pi R$ | 0.0977 | |

A continuous (not strobed) laser light sheet system in conjunction with smoke (propylene glycol), injected inside the settling chamber, was used to visualise the flow in planes parallel and perpendicular to the freestream.

The flow patterns, projected on a reference grid, were recorded on video and digitised on a computer. To bring out details, these images were enhanced by using traditional image processing techniques, such as contrast stretching, pseudo-coloring, filtering and contouring. Thus, enabling the determination of the location of the center of each disc edge vortex.

The experiment covers a range of $\bar{x}=x/R$ values between 1 and 4 in increments of 0.5. For more details the reader is referred to table 3.

**Table 3: Details of the experiment [9]**

| | $\mu$= 0.15 | | $\mu$= 0.23 | |
|---|---|---|---|---|
| Rotor speed | 2110 | RPM | 2110 | RPM |
| Tip speed | 190 | m/s | 190 | m/s |
| Thrust coeff. | 0.0064 | | 0.0064 | |
| Density | 1.209 | kg/m$^3$ | 1.197 | kg/m$^3$ |

Note that the disc angle of attack is unknown for both advance ratios, however since this angle will be small for both cases, it is set equal to zero for the verification.

3.2 Disc edge vortex lateral location

The lateral location $\bar{y}_c$ of both disc edge vortices is shown in figure 8 for $\mu$=0.15 and in figure 9 for $\mu$=0.23. From these figures one can see that the predicted location correlates satisfactory with the test data. This is especially true for the predicted location of the asymptotes for both disc edge vortices, which means that the calculated circulation distribution must be a reasonable approximation for the actual circulation distribution.

Note the part of both curves, inside the rotor disc. The progress of the rolling up process of both vortices is slightly to high, instead of following Kaden's solution to points inside the rotor disc, the vortices will follow its trailing edge till the solution lies outside the rotor.

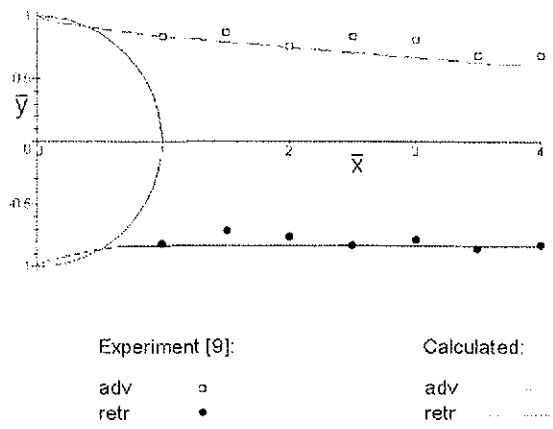


**Figure 8: Disc edge vortex lateral location, $\mu$=0.15**

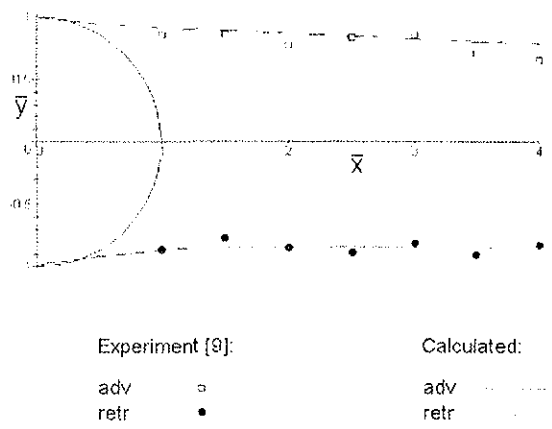


**Figure 9: Disc edge vortex lateral location, $\mu$=0.23**

From both figures it can be seen that the retreating disc edge vortex rolls up much faster than the advancing one. The distances behind the rotor where the disc edge vortices are fully formed, expressed as number of rotor radii, are

approximately:

| $\mu = 0.23$ | $\mu = 0.15$ |
|---|---|
| $\bar{e}_{adv} = 26.34$ | $\bar{e}_{adv} = 9.36$ |
| $\bar{e}_{retr} = 5.27$ | $\bar{e}_{retr} = 2.86$ |

The rather large difference between the distances needed for the advancing and retreating side disc edge vortex to roll up, is explained by the fact that the circulation is higher on the retreating side. Note that these numbers also show that the disc edge vortices will have a negligible influence on the tail rotor and tail sections for advance ratios $\mu \geq 0.15$. More experimental data is therefore needed to verify the model for lower advance ratios.

3.3 Disc edge vortex axial location

The axial location $\bar{z}_c$ of both disc edge vortices is shown in figure 10 for $\mu$=0.15 and in figure 11 for $\mu$=0.23. As for the predicted lateral location, the correlation with the test data is satisfactory.

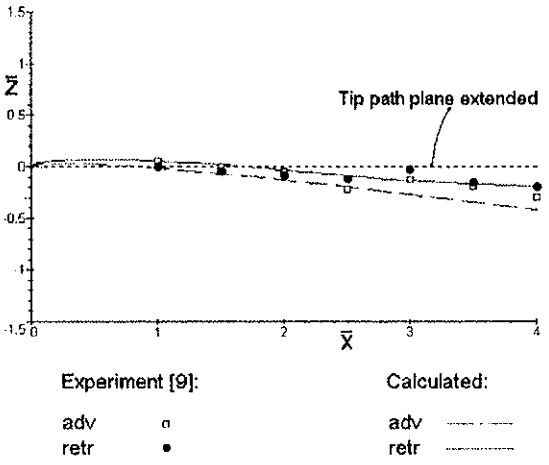


**Figure 10: Disc edge vortex axial location, $\mu$=0.15**

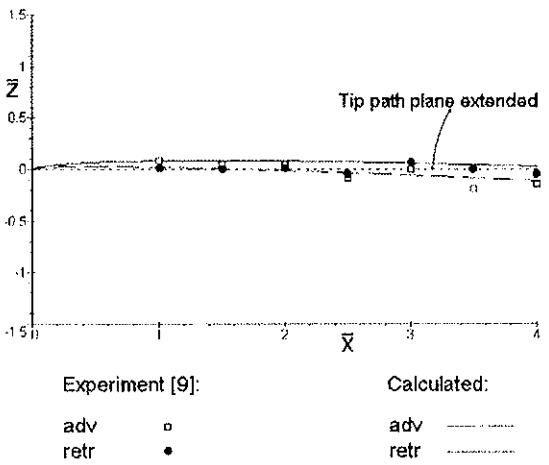


**Figure 11: Disc edge vortex axial location, $\mu$=0.23**

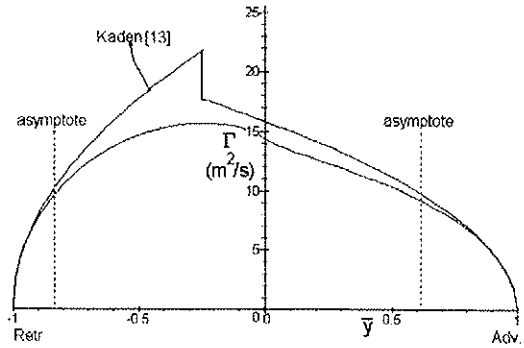


**Figure 12: Calculated circulation distribution, $\mu$=0.15**

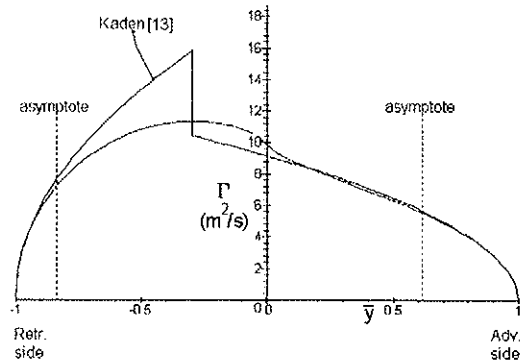


**Figure 13: Calculated circulation distribution, $\mu$=0.23**

In both cases it can be seen that the disc edge vortex on the advancing side lies below the retreating disc edge vortex. According to Ghee & Elliot, this is evidence for a stronger downwash on the advancing side. However, in the present model an inflow model is used that assumes just the opposite, i.e., downwash is stronger on the retreating side.

This controversy between inflow models in general and experimentally obtained downwash distributions, see for instance Baskin et al. [17], may be explained by the rolling up motion of the wake. In the model, this motion introduces an upward velocity component that subtracts from the induced velocity. On the retreating side the vortex rolls up much faster, apparently causing the resultant velocity to be smaller than on the advancing side.

3.4 Circulation distribution

In paragraph 3.2 it was shown that the asymptotes of both disc edge vortices are predicted correctly. So although it is not possible to verify the calculated circulation distribution directly, its shape must be approximately correct.

As can be seen in figure 12 and 13, the higher circulation is predicted on the retreating side. This is caused by the fact that the rotor is in moment equilibrium, therefore blade circulation must be higher on the retreating side than on the advancing side. Note that, Prouty [18] arrived at a circulation distribution that was similar in shape, which he

used to determine helicopter induced drag. However with the difference that the higher circulation was predicted on the advancing side. This cannot be true, because in this case the rotor is not in equilibrium. Furthermore, Prouty's distribution does not produce the correct asymptotic location of the disc edge vortices seen in the present model.

The rotor is trimmed,i.e., in moment equilibrium. This means that the circulation along a blade is higher on the retreating side than on the advancing side.

From figure 12 and 13, for $\mu$=0.15 and $\mu$=0.23 respectively, it can be seen that Kaden's approximation of the circulation distribution works well until the asymptotes are reached. This means that the approach proposed by Spreitner & Sacks for the fixed wing case, works just as well for a helicopter rotor.

3.5 Disc edge vortex geometry

Figure 14 gives a cross-section of both disc edge vortices at 3.5R behind the main rotor for $\mu$=0.15. Although there is no data to verify the actual shape of each disc edge vortex, they appear the same as the vortices encountered by Ghee & Elliot, see figure 15.

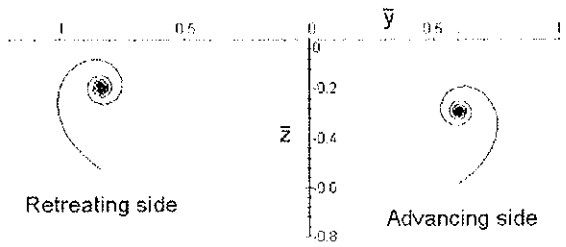


**Figure 14: Calculated geometry, $\bar{x}$=4 and $\mu$=0.15**

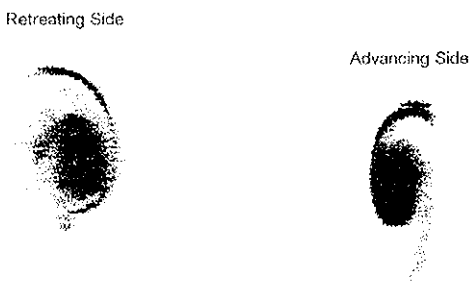


**Figure 15: Visualised geometry, data unknown [9]**

A strong vortex sucks in more air than a weak one. The suction of the retreating side vortex must therefore be greater than that of the advancing side vortex. Therefore less mass is transported into the advancing vortex, causing it to roll up more tightly. Note that Ghee and Elliot contribute this to the fact that the strength of the advancing side disc edge vortex is higher than that of the retreating vortex, but as discussed before this cannot be the case.

## 4 Conclusions

An analytical model has been derived to predict the location, strength and geometry of the disc edge vortices behind a helicopter rotor in low speed forward flight. The rotor has been redefined as an equivalent circular wing, and in turn the rolling up motion of its wake has been analysed with the help of a fixed wing theory developed by Kaden [13]. Important conclusions from this analysis are:

- The results obtained with the model compare reasonably well with the experimental results from Ghee & Elliot [9]. Both the lateral and axial location of the disc edge vortices are predicted with an accuracy acceptable for engineering purposes. The geometry of both vortices could only be compared qualitatively, but both their size and relative proportions seem to be correct. However, more data is needed to verify the model, especially for lower advance ratios $\mu \leq 0.15$.

- The advancing side disc edge vortex lies below the retreating side disc edge vortex, develops slower and is rolled up tighter. This is explained by the lower circulation on the advancing side, which determines the rate of the rolling up process and the suction of the vortex core. The disc edge vortex on the advancing side will therefore grow slower and, since less air is transported into it, it will have a smaller size. It will thus be located closer to the part of the sheet out of which it is formed. Though the induced velocities are lower on the advancing side, this results into a lower position for this vortex.

- The fully formed advancing side disc edge vortex is located closer to the rotor longitudinal axis of symmetry. The positions of the fully formed vortices can be related to the center of gravity of the vorticity distribution inside the undeformed sheet. The difference in the shape of the vorticity distribution, between the advancing and retreating side, therefore explains this asymmetry.

- All asymmetries, discussed above, become smaller with decreasing advance ratio.

- The relative position of both vortices can be seen as an indication of downwash strength. Which will therefore be lower on the retreating side than on the advancing side. This is a possible explanation for the difference between calculated induced velocities and experimentally determined downwash distributions.


## Acknowledgements

The author would like to thank the Faculty for Aerospace Engineering, of the Delft University of Technology, for the

funding and support of this work. He especially would like to acknowledge the invaluable contributions of Th. van Holten, K.P. Jessurun and J.A. Melkert.

References

1. Wiesner, W., and Kohler, G., *Tail Rotor Performance in Presence of Main Rotor, Ground and Winds*, Proceedings of the 29th Annual Forum of the American Helicopter Society, May 9-11 1983.

2. Hanker, E.J., and Smith, R.P., *Parameters Affecting Helicopter Interactional Aerodynamics in Ground Effect*, Presented at the 39th Annual Forum of the American Helicopter Society, May 9-11 1983.

3. Sheridan, P.F., Hanker, E.J. Jr., and Blake B.B., *A study of the Aerodynamic Interactions of the Tail Rotor and Fin*, Boeing Vertol Company, May 31 1983.

4. Ellin, Lt. Com. A.D.S., Royal Navy, *An in-Flight Investigation of Lynx AH MK5 Main Rotor Tail Rotor Interactions*, Proceedings of the 19th European Rotorcraft Forum, Cernobbio (Como), Italy, September 14-16 1993.

5. Srinivas, V., Chopra, I., Haas, D., and McCool, K., *Prediction of Yaw Control Effectiveness and Tail Rotor Loads*, Proceedings of the 19th European Rotorcraft Forum, Cernobbio (Como), Italy, September 14-16 1993.

6. Landgrebe, A.J., Bellinger, E.D., *An Investigation of the Quantitative Applicability of Model Helicopter Rotor Wake Patterns Obtained from a Water Tunnel*, USAAMRDL Technical Report 71-69, Eustis Directorate, U.S. Army Air Mobility Research and Development Laboratory, Fort Eustis, Virginia, December 1971.

7. Lehman, A.F., *Model Studies of Helicopter Rotor Flow Patterns in a Water Tunnel*, Proceedings of the 24th Annual Forum of the American Helicopter Society, Washington D.C., United States of America, May 8-10, 1968.

8. Heyson, H.H., *Analysis and Comparison with Theory of Flow-Field Measurements near a Lifting Rotor in the Langley Full-Scale Tunnel*, NACA TN 3691, 1956.

9. Ghee, A.T., and Elliot, W.J., *A study of the Rotor Wake of a Small-Scale Rotor Model in Forward Flight Using Laser Sheet Flow Visualisation with Comparison to Analytical Models*, Proceedings of the 48th Annual Forum of the American Helicopter Society, Washington D.C., United States of America, June 3-5, 1992.

10. Ormiston, R.A., *An Actuator Disc Theory for Rotor Wake induced Velocities*, AGARD - CPP 111, Sept. 1972.

11. Drees, J.M., *A Theory of the Airflow Through Rotors and Its Application to Some Helicopter Problems*, The Journal of the Helicopter Association of Great Britain, Vol. 3, No.2, July-Sept., 1949.

12. Bühler, M., and Newman, S.J., *The Aerodynamics of the Compound Helicopter Configuration*, Aeronautical Journal, April 1996.

13. Kaden, H., *Aufwicklung einer unstabilen Unstetigkeitsfläche*, Ingenieur-Archiv, band 2, Berlin, 1932.

14. Spreitner, J.R. and Sacks, A.H., *The Rolling Up of the Trailing Vortex Sheet and Its Effect on the Downwash Behind Wings*, Journal of the Aeronautical Sciences, volume 18, January 1951.

15. Heyson, H.H., *A Note on the Mean Value of Induced Velocity for a Helicopter Rotor*, NASA TN D-240, May 1960.

16. Durand, W.F., *Aerodynamic Theory*, Volume 2, Julius Springer, Berlin, 1935.

17. Baskin, V.Ye, Vil'dgrube, L.S., Vozhdayev, Ye.S. and Maykapar, G.I., *Theory of Lifting Airscrews*, NASA TTF-823, 1975.

18. Prouty, R.W., *Helicopter Performance, Stability and Control*, P.W.S. Publications, 1986.